Sensors & Transducers, Vol. 260, Issue 1, May 2023, pp. 7-13

www.sensorsportal.com

Sensors & Transducers

Published by IFSA Publishing, S. L., 2023
http://www.sensorsportal.com

Temperature Calibration of Twin Micro-heater Based Microcalorimeter

[1, *] Lajos HARASZTOSI, [1] István A. SZABÓ, [2] Ferenc BIRÓ, [1] Rebeka Gy. KISS and [1, 2] Gábor BATTISTIG

[1] University of Debrecen, Institute of Physics, 18/B Bem sqr., Debrecen, 4019 Hungary
[2] Centre for Energy Research, Institute for Technical Physics and Materials Science (MFA), Konkoly Thege M. str. 29-33, Budapest, 1121 Hungary
[1] Tel.: +36 52 512 900, fax: +36 52 316 073
[*] E-mail: lajos.harasztosi@science.unideb.hu

Received: 7 February 2023 Accepted: 5 April 2023 Published: 23 May 2023

Abstract: Calorimetry is often used as a material characterization method but needs large amounts of materials to be studied. Determination of reaction heat provides important information about the physical processes that take place during heating up the samples. Recently, the application of solid thin film structures became more important in various fields of surface sciences, microelectronics, coatings, etc. Microcalorimetry is an effective tool for investigating various thin film reactions. The volume of the materials needed for the measurements are limited. New micro-electromechanical membrane type silicon chip of twin micro heaters, electrical control system and temperature calibration method is developed and presented in this paper. The large temperature homogeneity of the heaters, the small volume of material needed for the studies and the sophisticated analog electronics provides a high-quality differential scanning calorimetry signal.

Keywords: Microcalorimetry, MEMS membrane structure, Microheaters, Signal processing, Temperature feedback and control

1. Introduction

Power compensated microcalorimeters can be utilized for the measurement of phase transformations or other sensing purposes [1]. A recent very detailed summary of microcalorimetry instrumentation and its applications can be found in [2]. Most of the literature of this subject focuses on the design and fabrication of microcalorimetry systems [3-6], the microheater/sample holder membrane structure [1,7], the operation of the driving and readout electronics [1, 8, 9] and the application of microcalorimetry to solve different physical or materials science problems [3, 7, 10-12].

The present work focuses on a specially designed membrane based micro-heater chip [13], which has two independent, but identical platinum heater elements with large temperature homogeneity over the heater surface. The sample and/or the reference material can be deposited onto the surface of one or both isolated microheaters. The preliminary results were presented at the SEIA 2022 conference [14].

The two independently controlled and power compensated elements are used to determine the power difference, i.e., the DSC (Differential Scanning Calorimetry) signal. A novel two channel analog electronics and control software is developed and presented here. The new measuring system allows us

to record and calibrate the temperature scale of the DSC signal with high precision.

Several approaches are used for the calibration of microcalorimeters. In [15] a MEMS type DSC microcalorimeter using a thermopile for temperature sensing is presented. The calibration was performed by observing the well-established melting points of several alloys: In (156.6 °C), Sn (231.9 °C), Pb (327 °C) and Ge/Al eutectic (449.5 °C). The calibration procedure of the NIST MEMS nanocalorimeter, which uses a Pt film heather/sensor element is described in [16]. They have shown that the self-heating effect of the MEMS sensor must be considered even for low applied currents.

2. Microcalorimeter MEMS Sensor

Full membrane twin micro-heater platform designed for calorimetric gas sensors in ambient air operation [13], was adopted for the microcalorimetry application. The sensor chip is presented in Fig. 1. The 150 μm diameter annular shaped platinum filament embedded in 20 - 20 nm TiO_x layers was fabricated from 400 nm thick platinum film by RIE (Reactive Ion Etching) process on a SiO_2 - Si_3N_4 multilayer membrane and covered with 300 nm SiO_2. The thicknesses of the individual layers were selected such as to provide reduced mechanical stress in the membrane. The heating filament of the microheater is made up of sections of constant thickness, variable width, and geometry. Filaments are connected in series, thus a homogeneous temperature distribution can be ensured. Dimensions of the outer ring and the inner rings of the filament were designed to maintain uniform temperature distribution with ± 1 – 3 % difference in the temperature range of 100 – 850 °C over the entire filament [17].

The filaments are powered through 220 μm long interconnections, furthermore four-point contacts were adopted to ensure accurate filament resistance measurement. Anisotropic wet silicon etching was used at the backside of the wafer to form the cavity and release the membranes with c.c. 380 × 590 μm^2. The temperature of the membrane based microheater is determined by the precise measurement of the resistance change of the Pt filament during heating. The Temperature Coefficient of Resistance (TCR) of the platinum filament was found to be 2.85×10^{-3} 1/°C, measured up to 500 °C.

Thermal homogeneity over the surface is an essential point of scanning microcalorimetry. During the measurement the sample temperature is varied between room temperature and maximum temperature, in our experiments between 22 °C – 350 °C. within seconds or even faster. Due to the low thermal mass and the good thermal isolation, the bare microheater can be heated up to the operation temperature in the millisecond range. 30 mW heating power provides 450 °C. The local temperature of the different parts of the material to be studied could be seriously different because of the inhomogeneity of the heating. Hence the solid-state reaction of the parts of the matter could take place in different times. In this case the DSC signal the corresponding peak will appear as a wider but less intensive peak. In this case the exact temperature and the reaction heat of the solid-state reaction cannot be identified.

The advantage of the direct measurement of the temperature through the resistance of the filament in comparison to the separated temperature sensor integrated on the chip is that the real temperature at the sample position can be monitored by minimizing the effects of thermal conduction and convection over the chip.

The heat conduction is also minimized as the Pt heater is embedded in a SiO_2/Si_3N_4 dielectric thin membrane over a large cavity. The Si body of the chip is quite far away, only the very thin current and voltage line can conduct very limited heat from the heated surface to the large bulk.

Thin sample and/or reference films were deposited onto the surface of the microheaters of 150 μm diameter. Silicon hole mask manufactured by deep reactive ion etching was applied as a mask for the thermal evaporation. In this work, for testing the measurement system, 200 nm thick In and Sn films of the diameter of 150 nm were deposited.

3. Microcalorimeter Development

The electrical contacts of the heating element can be seen in Fig.1 (b). The Pt resistor is heated by a current source and the actual voltage on it can be measured. So as to neglect the effect of additional voltage drop on the current wires, a four-wire heating element is realized.

The measurement system (Fig. 2) contains two independent, identical analog channels, each realizing an analog control loop. The two control loops are individually driven by two separated DA converters. This setup gives the capability - by applying slightly different signal levels - of taking care of the difference on the two control loop electronics and Pt heater-sample systems. The control system keeps the heating elements at the same temperature set by the computer during the full process. The difference of the required power of the heaters, contains the information about the heat of transformation of the sample.

Two independent analog control loops are realized for driving the heating elements. On Fig.3 the block diagram of the control loop is shown. One channel for the reference (with or without reference material) and the other for the sample is developed.

The temperature of the heating element is determined by its resistance in the control loop.

Calculation of the resistance is made by the mathematical division of the voltage on the heating element by the voltage related to the current on it. The circuit on Fig. 4. makes the analog division task.

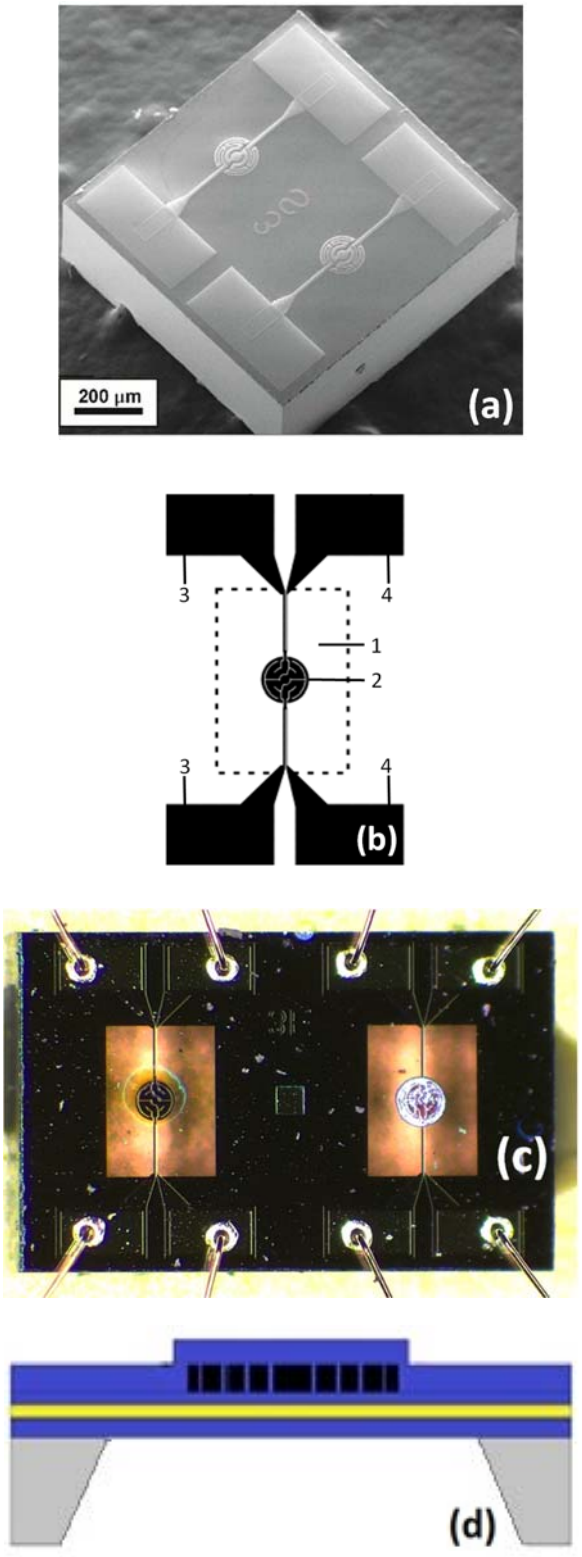

Fig. 1. SEM image (a) of the micro-heater chip fabricated by Si bulk micromachining. Two embedded Pt heaters are formed into the membrane structure. Electrical connections of a microheater (b): 1 membrane, 2 Pt microheater, 3 current and 4 voltage contacts. (c) optical image of the mounted chip, the heater on the right side is covered by a thin film of In. The bright area around the circular heater is the ≈ 1 mm thick dielectric self-supported membrane (back side illumination). (d) The cross section of the microheater: SiO_2 - blue, Si3N4 - yellow, Pt - black, c-Si - grey (d).

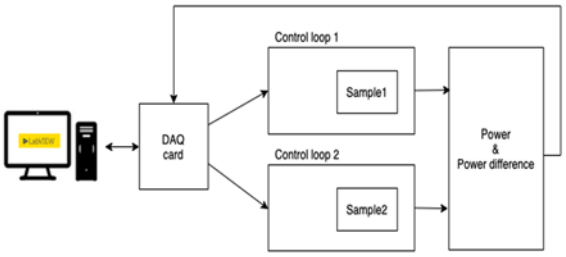

Fig. 2. The scheme of the realized measurement system.

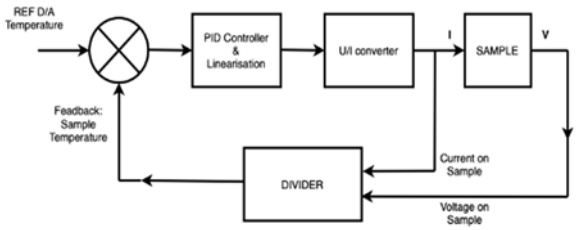

Fig. 3. Analog temperature control loop.

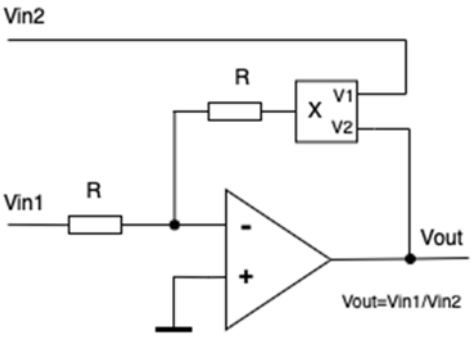

Fig. 4. The divider amplifier.

The divider circuit is based on an inverting amplifier stage and realizes the function by using analog multiplier in the feedback loop. The V_{in1} voltage can be bipolar, but V_{in2} must only be positive. In addition, the V_{in2} must not be too small, because the resulted V_{out} signal level will to high and will be saturated at the maximal output level of the operational amplifier.

The resistance is linearly proportional to the temperature of the heating element as the TCR of the Pt heater is constant below approx. 500 °C. The input power, i.e., the temperature of the heater element is set by a PID type controller. The power applied to the heater is proportional to the square of the driver current, so it makes the system transfer function nonlinear. In order to make the control system linear, a square root function is used to linearize the whole system transfer characteristic. The principle of the realization of the square root function is the inverse function realization method, seen on the Fig. 5. In the basic inverting amplifier feedback loop there is a square function network realized by an analog multiplier, so the whole transfer function of the circuit

realizes the analog square mathematical equation. The circuit works fine only in the negative voltage range of the input voltage, till its zero value. (The inverting configuration inverts the negative input voltage to positive at the output, so at the inverting point of the operational amplifier the two currents of the resistors cancel each other.)

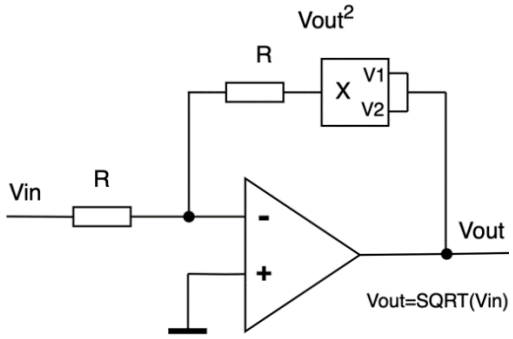

Fig. 5. Analog square root amplifier stage.

In order not to let the Vin to be negative, a limiter circuit must also be applied.

The tiny Pt heating elements are very sensitive to the driving current: the maximum current applied on our device should be below 25 mA. At maximum continuous current the temperature of the heater is around 600 °C. Above this current limit the device may be damaged. In pulsed current operation mode however, the temperature of the heater can reach and withstand 1000 °C. Another problem arises related to the analog divider, when the denominator becomes too close to zero, its output signal becomes too high and saturates the divider amplifier stage output. The solution to both previous problems is to insert a limiter network in front of the current source.

The transfer function of the limiter can be seen on Fig. 6.

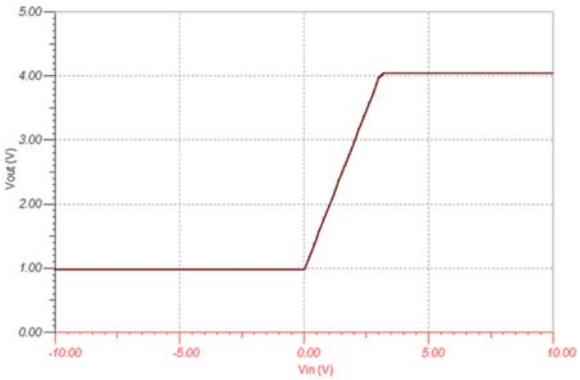

Fig. 6. Analog limiter circuit transfer function.

As it was mentioned earlier, there are minimum and maximum limits as well, but between the limits, the transfer function must be precisely linear, with sharp transition regions nearby the knee points.

Even at lower voltage levels, there is a minimal current which heats up the Pt heaters. This means, of course, that we can't start the measurement from room temperature. This preheating temperature is about 60 □ in our system, so it does not significantly reduce the possible applications. On Fig.8. the measurement starts at approx. 80 □. This preheated state of the heating Pt elements blocks the determination of the room temperature resistivities, so this measurement is made prior to placing the sensors into the measurement setup and the values are set into the software as parameters.

Analog electronics always contain offset, gain, linearity, and temperature drift errors. These errors must be minimized by selecting proper circuit solutions and components, but despite this, cannot be fully eliminated. To manage the residual error content, the transfer functions of all the system blocks are carefully determined. The offset and gain error parameters are compensated in the control software. The linearity of the applied amplifiers is very high (-120 dB minimum) and the drift parameters are very low (1 μV/°C maximum), so there is no need for compensating them.

One of the analog control loop electronics can be seen on Fig. 7.

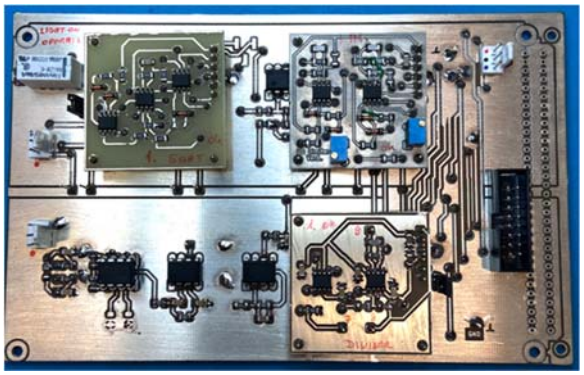

Fig. 7. Analog control loop electronics.

The electronics uses a base board (Europe card size) and three small PCB modules, related to different block diagram functions. It also contains a protection relay, which lets the electronics to be connected to the sample only after the powering up, so the initial transients cannot destroy the tiny sample.

4. Instrumentation and Calibration

The hardware is controlled by a National Instruments USB6212 data acquisition card. The two DA output channels provide the reference signals for the analog controller. The main measured quantities are the power, resistance values and the power difference. The control software was developed in LabVIEW (Fig. 8).

The user interface provides the possibility to setup the measurement, perform the calibration, and display and save the results. There is a sequence of steps, which must be followed. As each sensors have slightly different geometrical parameters, the resistances of the two sensors are different. On Fig. 8 the main user interface of the LabVIEW code can be seen.

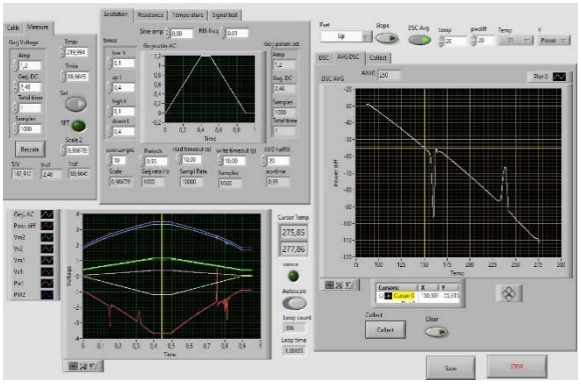

Fig. 8. Front panel of the LabVIEW control software - driving voltage (left upper), resistance and power applied on both heater (left bottom) and DSC signal (right middle).

The calibration process starts with the determination of the room temperature resistances of the heater elements. This is performed with an HP-34401A multimeter using the four-point resistance measurement mode. The measurement was done in a thermally isolated chamber. The temperature was measured with a precision thermometer. The excitation current was kept low by manually selecting a high resistance measurement range (0.1 mA), which creates a negligible self-heating effect [16]. The two cells usually have a slight, but not negligible resistance difference, which should be taken into account during the DSC measurements. The platinum films are used both as the heater and the temperature sensor. We assumed a linear temperature dependence for both resistors within the operational range of the DSC.

We assume, that the temperature coefficient is the same, but might be slightly different from the bulk value of the platinum. Platinum films are used both as the heater and the temperature sensor. We calculated with a linear temperature dependence for both resistors within the operational range of the DSC (eq.1-2).

$$R^1 = R_0^1\big(1 + \alpha(T - T_0)\big) \quad (1)$$

$$R^2 = R_0^2\big(1 + \alpha(T - T_0)\big) \quad (2)$$

where T_0 is the room temperature, α is the Temperature Coefficient of Resistance (TCR) of platinum, R_0^1 and R_0^2 are the room temperature resistance of the microheaters, R^1 and R^2 are the resistance of the platinum heaters at temperature T.

As the feedback is based on a voltage proportional to the resistance to the heater, we must use different reference voltages for the two controller loops to reach the same temperature. The ratio of the resistances is independent of the temperature and can be set by requiring the two cells to reach the same measured maximal temperature. The two reference voltages are proportional to each other, the ratio is equal to the ratio of the room temperature resistances. These two steps ensure that the two calorimeters are in the same temperature range during the measurement.

The linear temperature coefficient of the platinum heaters was determined in a separate experiment. For this, we applied special calibration samples where thin metal layers of In and Sn were deposited on the Pt heaters. In the power difference curve these peaks will appear with different signs relative to the baseline. The temperature calibration was performed by the observation of the melting temperatures of these alloys at different heating rates [15] (Fig. 9).

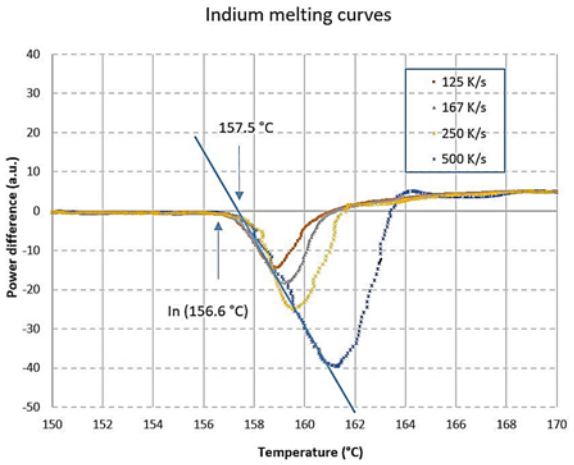

Fig. 9. Melting curves for In before calibration. The horizontal axis is the uncalibrated temperature scale in °C. The vertical axis is the power difference. The heating rates are 500 K/s, 250 K/s, 167 K/s and 125 K/s.

The peak temperature shifts to higher values for larger heating rates, but the onset temperature remains nearly the same for both In and Sb. The onset of melting temperature was determined based on the slowest heating rate, and the temperature coefficient was changed to receive the reference values for the samples In (156.6 °C) and Sn (231.9 °C) (Fig. 10).

After the determination of the temperature coefficient α, the same value can be used for the other DSC chips. The only parameter, which must be determined are room temperature resistance values R_0^1 and R_0^2 .

Once the temperature scale is calibrated, one can perform measurements under different conditions. The temperature profile consists of three parts. First, the sample is kept at a lower temperature, where there is no transformation to reach equilibrium. Next, the sample is heated linearly up to the end temperature, which is above the region of transformation. After keeping the sample at the higher temperature for a certain time, the steps are repeated in the other direction.

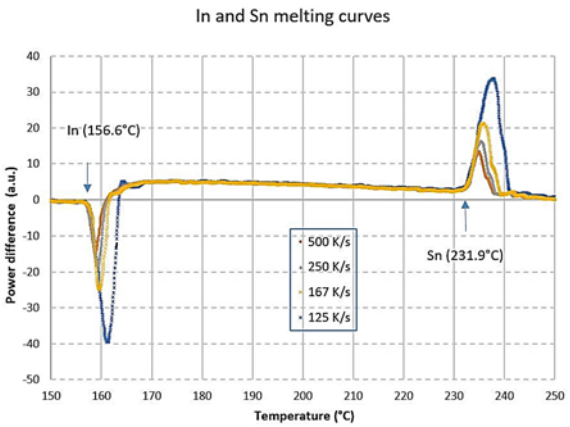

Fig. 10. Melting curves for In and Sn for the different heating rates after calibration. The vertical axis is the recorded power difference. The heating rates are 500 K/s, 250 K/s, 167 K/s and 125 K/s.

For development purposes all the raw signals are also displayed by the program, The final result of the measurement is the graph of the power difference of the two sides as a function of the temperature. There is a possibility to do a linear baseline correction for better visualization of the results. The final analysis of the data is performed manually based on the measured data points.

5. Conclusions

A novel differential micro calorimeter system, based on MEMS membrane type heater elements was developed. The present solution has several advantages over the previous works like the homogeneity of the temperature over the heated elements and the fast analog linearized feedback control system. The use of microheater chips as a substrate to deposit the investigated thin film structure has the major advantage: chips as they produced by microtechnology, the associated coast per chip is very low. Si shadow mask needs to locally deposit the thin film structures is also fabricated by microtechnology. Mask can be reused after a deposition circle without any further cleaning. By using two well-known metal thin film materials, accurate temperature calibration is realized. By using other metal thin films, the accuracy of the temperature calibration can be further increased. In the near future, we intend to use the developed DSC measurement system to investigate new thin-layer physical problems. The reaction heat of first and second order phase transitions on multilayer thin film structures are going to be determined.

Acknowledgements

Work was partially supported by TKP-2019-21 and TKP2021-NVA-03 research projects of the Ministry of Innovation and Technology of Hungary from the National Research, Development and Innovation Fund.

References

[1]. A. F. Lopeandia, J. Valenzuela, J. Rodriguez-Viejo, Power compensated thin film calorimetry at fast heating rates, *Sensors and Actuators A Physical,* Vol. 143, Issue 2, 2008, pp. 256–264.

[2]. T. Y. Gao, B. Zhao, J. J. Vlassak C. Schick, Nanocalorimetry: Door opened for in situ material characterization under extreme non-equilibrium conditions, *Progress in Materials Science*, Vol 120, 2021, p. 100819.

[3]. P. J. McCluskey, J. J. Vlassak, Combinatorial nanocalorimetry, *J. Mater. Res.,* 25, 2010, 2086.

[4]. M. Merzlyakov, Method of rapid (100 000 K s−1) controlled cooling and heating of thin samples, *Thermochimica Acta,* 442, 2006, pp. 52–60.

[5]. A. F. Lopeandía, Development of Membrane-based Calorimeters to Measure Phase Transitions at the Nanoscale, Thesis, Grup de Nanomaterials i Microsistemes, Departament de Física, *Universitat Autònoma de Barcelona*, Bellaterra, May 2007.

[6]. F. Yi, M. D. Grapes, D. A. LaVan, Practical Guide to the Design, Fabrication, and Calibration of NIST Nanocalorimeters, *Journal of Research of the National Institute of Standards and Technology*, Vol. 124, 2019, Art. 124021.

[7]. V. Mathot, M. Pyda, T. Pijpers, G. Vanden Poel, E. van de Kerkhoff, S. van Herwaardeng, F. van Herwaardeng, A. Leenaers, The Flash DSC 1, a power compensation twin-type, chip-based fast scanning calorimeter (FSC): First findings on polymers, *Thermochimica Acta,* 522, 2011, pp. 36–45.

[8]. E. Zhuravlev, C. Schick, Fast scanning power compensated differential scanning nano-calorimeter: 1. The device, *Thermochimica Acta,* 505, 2010, pp. 1–13.

[9]. E. Zhuravlev, C. Schick, Fast scanning power compensated differential scanning nano-calorimeter: 2. Heat capacity analysis, *Thermochimica Acta*, 505, 2010, pp. 14-21.

[10]. J. Zheng, Y. Miao, H. Zhang, S. Chen, D. Lee, R. Arroyave, J. J. Vlassak, Phase transformations in equiatomic CuZr shape memory thin films analyzed by differential nanocalorimetry, *Acta Materialia*, 159, 2018, pp. 320-331.

[11]. D. W. Denlinger, E. N. Abarra, Kimberly Allen, P. W. Rooney, M. T. Messer, S. K. Watson, F. Hellman, Thin film microcalorimeter for heat capacity measurements from 1.5 to 800 K, *Rev. Sci. Instrum.*, 65, 1994, p. 946.

[12]. D. Lee, J. J. Vlassak, Diffusion kinetics in binary CuZr and NiZr alloys in the super-cooled liquid and glass states studied by nanocalorimetry, *Scripta Materialia,* 165, 2019, pp. 73–77.

[13]. F. Bíró, Z. Hajnal, I. Bársony, Cs. Dücső, MEMS Microhotplate Constraints, in Advances in Microelectronics: Reviews, Volume 2, Sergey, Y. Yurish (Ed.), *IFSA Publishing*, Spain, 2019, pp. 49-67.

[14] L. Harasztosi, I. A. Szabó, F. Biró, R. Gy. Kiss and G. Battistig, Microcalorimeter development and calibration based on a twin micro-heater platform, in *Proceedings of the 8th International Conference on*

Sensors and Electronic Instrumentation Advances (SEIA' 2022), Corfu, Greece, 2022, pp. 112-116.
[15]. L. P. Cook, R. E. Cavicchi, M. L. Green, C. B. Montgomery, and W. F. Egelhoff, Thin□Film Nanocalorimetry: A New Approach to the Evaluation of Interfacial Stability for Nanoelectronic Applications, *AIP Conference Proceedings*, 931, 2007, pp. 151–155.
[16]. Feng Yi, Michael D. Grapes and David A. LaVan, Practical Guide to the Design, Fabrication, and Calibration of NIST Nanocalorimeters, *Journal of Research of the National Institute of Standards and Technology*, Vol. 124, 2019, Art. 124021.
[17]. Patent: HU 5279, U2000150
